Journal of Industrial and Engineering Chemistry 53 (2017) 68–76

Contents lists available at ScienceDirect

Journal of Industrial and Engineering Chemistry

journal homepage: www.elsevier.com/locate/jiec

Improved performance of flexible polymer light emitting diodes with an indium-zinc-tin-oxide transparent anode by controlling the thermal treatment temperature

Soo Won Heo[a], Eui Jin Lee[b], Yong Woon Han[b], Yo Seb Lee[c], Won Jae Lee[c], Sung-Hoon Choa[c], Young Sung Kim[c], Doo Kyung Moon[b,*]

[a] RIKEN Center for Emergent Matter Science (CEMS), 2-1 Hirosawa, Wako,Saitama 351-0198, Japan
[b] Department of Materials Chemistry and Engineering, Konkuk University, 120, Neungdong-ro, Gwangjin-gu, Seoul 05029, Republic of Korea
[c] Graduate School of NID Fusion Technology, Seoul National University of Science and Technology, 232 Gongneung-ro, Nowon-gu, Seoul 01811, Republic of Korea

ARTICLE INFO

Article history:
Received 17 January 2017
Received in revised form 20 March 2017
Accepted 25 March 2017
Available online 4 April 2017

Keywords:
Flexible transparent electrode
Flexible polymer light emitting diodes
IZTO transparent electrode

ABSTRACT

The indium-zinc-tin-oxide (IZTO) target, which consisted of 70 at.% In_2O_3– 15 at.% ZnO^- 15 at.% SnO_2, was manufactured to replace indium-tin-oxide (ITO). The flexible IZTO (FIZTO) transparent electrodes were deposited on polyimide (PI) films at temperatures ranging from room temperature to 300 °C. The mechanical, optical and electrical properties of the FIZTO films and the flexible polymer light emitting diodes (FPLEDs) were characterized. Amorphous FIZTO prepared at 50 °C showed the best performance. The optimized FPLEDs exhibited 31% and 9% enhanced maximum brightness and luminance efficiency, respectively, as compared to PLEDs with an ITO glass. In addition, the FPLEDs worked normally in the stretching and twisting state at 3.2% and 58°, respectively.

Introduction

Optoelectronic devices such as organic (polymer) light emitting diodes (OLEDs and PLEDs) [1–4], touch screen panels (TSPs) [5], quantum dot solar cells (QDSCs) [6,7], and organic photovoltaic cells (OPVs) [8–11] have attracted significant attention as the next-generation flexible electronic devices (FEDs) that can enhance productivity by continuous processing. For high-efficiency FEDs, it is necessary to increase the performance of the active matrix and enhance its chemical and mechanical stability. In addition, advanced encapsulation technology is required to protect the active matrix. Recently, a number of studies have also been conducted on the development of transparent conducting electrodes (TCEs) which maintain a high level of transmittance, conductivity, and flexibility for the commercialization of FEDs. In general, ITO is the most common choice for a transparent conducting electrode (TCE) material, owing to its advantages of low resistivity and high transparency in the visible wavelength region [12–14]. Demand for ITO as an essential component in a wide range of industrial applications including flat panel displays, solid-state lighting, solar cells, and e-paper is rapidly increasing.

However, ITO has major drawbacks with respect to its properties and costs [15]. It is a ceramic material that cracks and fractures at low strains (2–3%) [16]. In addition, salt, acid, or device adhesives that are commonly found in nature corrode the ITO electrode and reduce the lifetime of the devices [17,18]. Further, the high-cost ingredient of the ITO, 'indium' and the deposition process are the biggest obstacles in using ITO as the TCE for FEDs. Because of the high deposition temperature and the low glass transition temperature (T_g) of the plastic substrate, it is difficult to apply the ITO to the flexible device [19]. Therefore, it is necessary to reduce the processing-temperature, the low-resistance, and high-transparency indium, or develop technologies for indium-free transparent electrodes [20–23].

TCEs can be developed into one-dimensional structures such as CNTs, graphene nanoribbons, metal nanowires, and nanowires of oxides. However, they have the disadvantage of low flexibility [24–26]. In addition, continuous structure films such as fluorine-doped tin oxide including ITO, novel oxide, metal thin films, large-area graphene, and conducting polymer require complicated and high processing temperatures. Among these oxide continuous films, indium zinc tin oxide (IZTO) with a reduced indium content,

* Corresponding author.
E-mail address: dkmoon@konkuk.ac.kr (D.K. Moon).

http://dx.doi.org/10.1016/j.jiec.2017.03.050
1226-086X/

containing ZnO has emerged as a leading alternative to ITO [27–29]. In spite of low deposition temperatures, the IZTO maintains a high work function, low resistivity, low sheet resistance and a high transmittance. Therefore, it can be applied onto the plastic substrate, making the fabrication of flexible devices possible [30].

Oxide continuous film TCEs are usually fabricated using the magnetron sputtering system. Because properties of them are sensitive to the deposition conditions, which are deposition power, gas pressure, composition of gas contents and processing temperature of the sputtering system, the optimization of deposition conditions is highly important. In our previous study, we had discussed the effects of oxygen partial pressure on electrical resistivity, optical transmittance of the IZTO and the PLED fabricated on the IZTO using a glass substrate [30]. However, studies have not been conducted to investigate the electrical, optical, and structural properties of the IZTO thin film prepared on a plastic substrate under variations in processing temperature.

In this study, therefore, IZTO TCEs comprising of In_2O_3 (70 at.%), ZnO (15 at.%) and SnO_2 (15 at.%) were fabricated as the IZTO target. After fixing the oxygen flow rate at 3%, the IZTO TCEs were fabricated under diverse deposition temperature conditions ranging from room temperature (RT) to 250 °C, and then their properties were analysed. To check the behaviour of IZTO at high thermal treatment conditions, colourless polyimide (PI) with a high thermal resistance was used as the plastic substrate. Then, the chemical binding state and the work function of the surface, that have a major effect on the characteristics of the FEDs and the optimum deposition conditions were measured through X-ray photoelectron spectroscopy (XPS) and ultraviolet photoemission spectroscopy (UPS). In addition, optimized IZTO thin films were introduced as flexible TCE, and flexible PLEDs that have generated attention as the next-generation FEDs, were fabricated and characterized.

Experimental section

Deposition and characterization of IZTO thin films on a polyimide (PI) substrate

By using pulsed DC magnetron sputter at an oxygen flow rate of 3% with deposition temperature range of room temperature ~200 °C, the IZTO films were deposited on a PI film (Mitsubishi gas chemical, 100 μm, Japan). The target were of the composition 70 at.% In_2O_3 15 at.% ZnO^- 15 at.% SnO_2. The PI substrate was washed by ultrasonication with detergent (10 wt% in water), acetone, isopropyl alcohol, and de-ionized water in sequence. The substrates were dried by blowing N_2 gas and baked at 120 °C hot plate. The cleaned PI substrates were loaded in the sputtering chamber. Sputtering was carried out with 125 W input power, 30 kHz frequency and 6 mTorr oxygen partial pressure whose flow ratio was 3% [O_2/(O_2 + Ar)]. The thickness of the deposited IZTO films was 200 nm.

The X-ray diffraction (XRD) patterns of IZTO films were analysed by Rigaku D/MAX 2200 diffractometre with Cu Kα radiation. Focused ion beam (FIB; NOVA600 NanoLab, FEI, Holland) through STEM (JEM-2100(HR) + Cs corrector, JEOL/CEOS, Japan) technic was processed for sample preparation and crystal phase was reviewed. Atomic force microscopy (AFM; XE-100, Park systems, Korea) and field emission scanning electron microscopy (FESEM; S-4800, HITACHI, Japan) were used to characterize surface morphology of IZTO films. The thickness of all prepared films was measured by an Alpha step 500 surface profiler (KLA-Tencor, USA). The electrical properties which are the resistivity, carrier concentration, and the mobility of the IZTO films were characterized by using the van der Pauw method with a Hall measurement system (HMS-3000, ECOPIA, Korea). The transmittance of the transparent anodes was measured by a UV-visible spectrometre (HP Agilent 8453, USA). The surface chemical state and work function of films were analysed by X-ray photoelectron spectroscopy (XPS; ESCA 2000, VG Microtech, UK) and UPS (He I, $h\nu$ = 21.22 eV, AXIS-NOVA, Kratos Inc., UK).

Fabrication and characterization of the flexible PLEDs with an IZTO transparent anode

To clean the surface of IZTO/PI, ultrasonification was performed in detergent (Alconox© in deionized water, 10 wt%), isopropyl alcohol (IPA), and deionized water for 1 min in sequence. After cleaning, moisture was completely removed by blowing N_2 gas and baking at 110 °C hot plate for 10 min. The IZTO transparent electrodes were ultra-violet ozone (UVO) treated for 10 min. For emitting layer, SPG-01T (green emitting polymer, Merck, Germany) was dissolved in chlorobenzene with concentration of 0.5 mg/ml and filtered through a 0.45 μm PTFE syringe filter. The emitting layer was coated to an 80 nm thickness and annealed at 90 °C for 30 min to remove the residual solvents. The electron transport layer and cathode were deposited thermally in a high vacuum chamber ($<1 \times 10^{-6}$ Torr) in the order of BaF_2 (0.1 Å/s, 2 nm), Ba (0.2 Å/s, 2 nm), and Al (5 Å/s, 200 nm). The performance of the PLEDs was characterized by using a Keithley 2400 source metre unit (Keithley, USA) and a PR 670 spectra scan (Photo Research, USA).

Results and discussion

Fig. 1 shows the XRD patterns of the FIZTO film deposited by pulsed DC magnetron sputtering. The films were deposited at various temperatures from RT to 300 °C with an oxygen partial pressure of 3%. The sample exhibited an amorphous structure with a weak and broad peak (2θ = ~31°) in the temperature range RT–150 °C. However, when the deposition temperature was 200 °C or higher, crystallization occurred. In case of SnO_2-doped In_2O_3 (ITO) thin films, in general, low amorphous and crystalline transition temperatures are found. Therefore, rapid crystallization takes place even at low substrate temperatures (RT–150 °C). In case of ZnO-doped In_2O_3 (IZO) thin films, however, higher amorphous and crystalline transition temperatures are found. Therefore, the amorphous structure remains stable until approximately 500 °C [31]. The FIZTO films have a stable amorphous structure similar to the IZO film because of the immiscibility of SnO_2 and ZnO in In_2O_3. ITO thin films fabricated at room temperature normally exhibit (222) orientations of crystalline structure because of surface heating caused by plasma irradiation during sputtering. In this

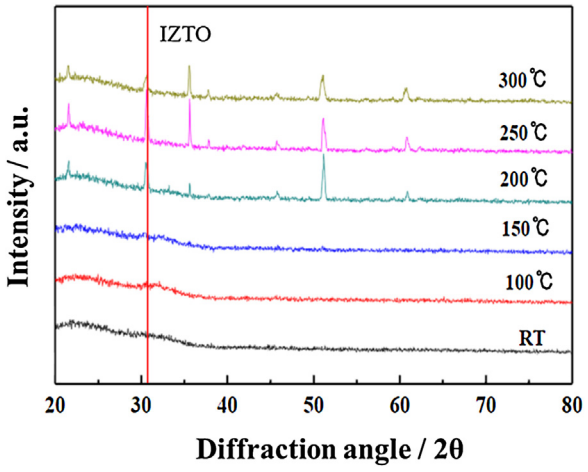

Fig. 1. X-ray diffraction patterns of IZTO films with various deposition temperatures on a PI substrate.

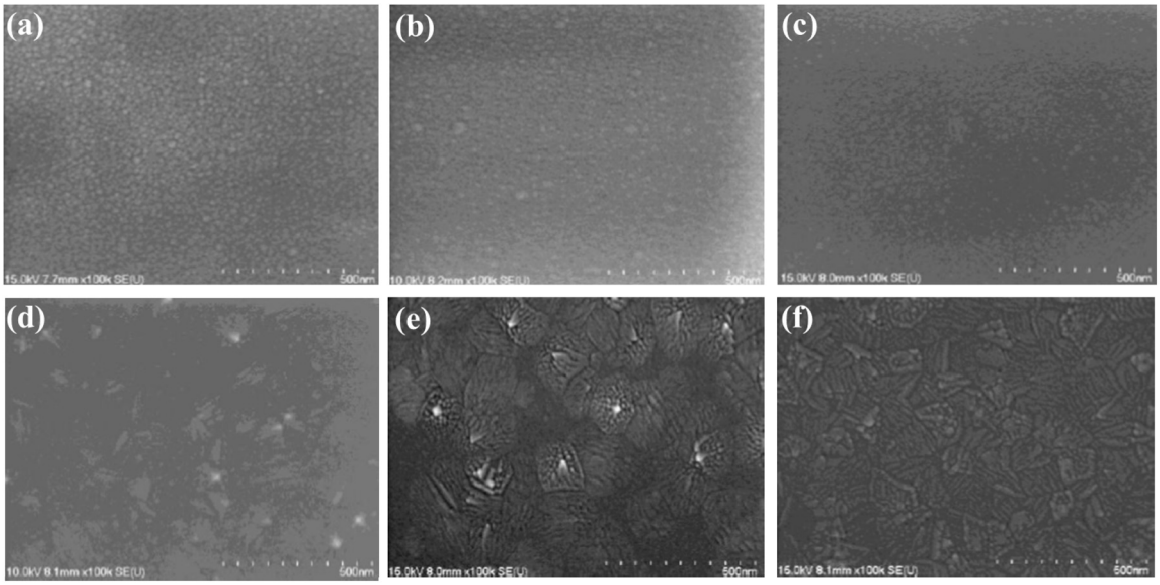

Fig. 2. FESEM images of IZTO films with various deposition temperatures, (a) RT, (b) 100 °C, (c) 150 °C, (d) 200 °C, (e) 250 °C, and (f) 300 °C.

study, the FIZTO films demonstrated a stable amorphous structure at temperatures below 200 °C owing to their significant thermal stability.

The surface morphology of the FIZTO films deposited on PI substrates at various temperatures was characterized using FESEM, and the results are presented in Fig. 2. As shown in (Fig. 2(a)–(c)), the FIZTO films exhibited a stable amorphous structure without defects such as pinholes, cracks or protrusions in the temperature range from RT–150 °C with highly smooth surfaces. In agreement with the XRD patterns shown in Fig. 1, the surface state of the FIZTO films also retained its amorphous structure even after the temperature increased to 150 °C. However, the transition to partially poly-crystalline occurred at 200 °C (Fig. 2(d)), and the film becomes fully crystalline at over 250 °C (Fig. 2(e)–(f)), indicating a preferred orientation similar to that exhibited by an ITO thin film.

The surface roughness of the IZTO thin films fabricated at different deposition temperatures was measured using the AFM, and the results are shown in Fig. 3 below. As expected, the RMS value in the temperature range RT–150 °C was 1.0 nm or below. Compared to the ITO thin film (Fig. 3(f)) with a 1.84 nm of RMS, a relatively smooth surface was found. However, when the deposition temperature was 200 °C or above, poly-crystalline structures were also found in the IZTO, revealing a rough surface morphology. Therefore, the IZTO thin film has a low RMS value because of higher thermal stability below 200 °C, compared to the ITO.

The microstructural analysis of the crystallized IZTO thin film deposited under an optimal condition (150 °C) was performed using cross-sectional high resolution transmission electron microscopy (HRTEM). The HRTEM image and selected area electron diffraction (SAED) patterns are shown in the inset of Fig. 4(a). The uniform contrast observed in the HRTEM image

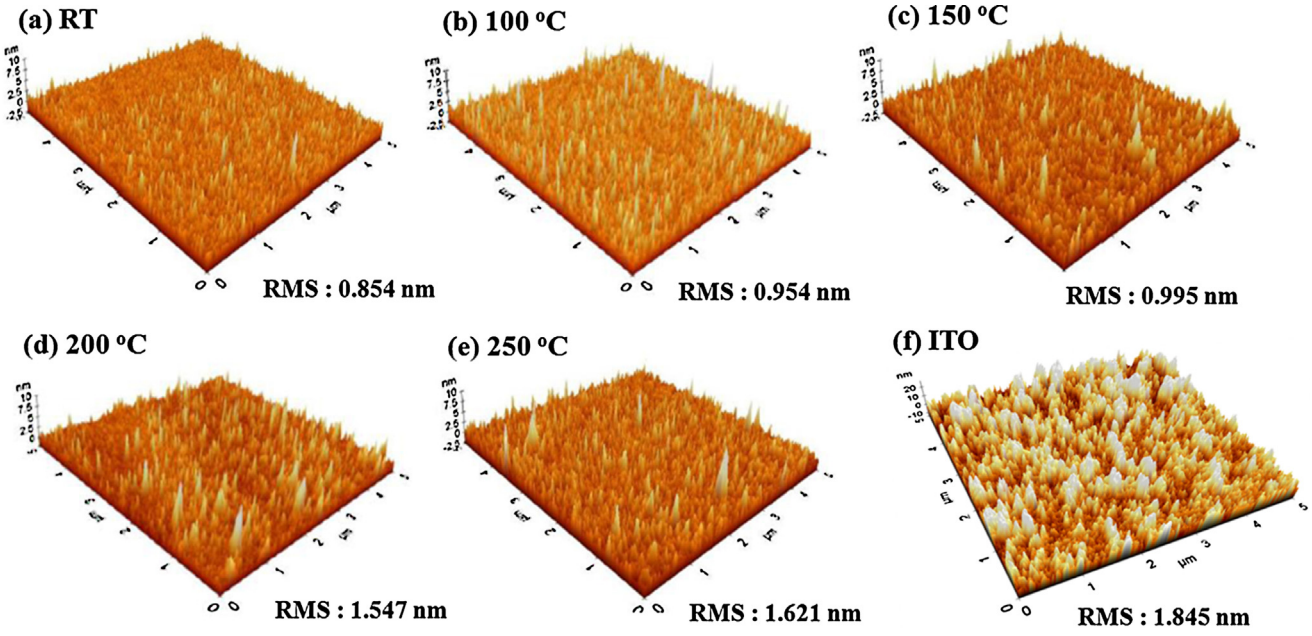

Fig. 3. AFM images and surface roughness of the IZTO films with various deposition temperatures, (a) RT, (b) 100 °C, (c) 150 °C, (d) 200 °C, (e) 250 °C, and (f) reference ITO.

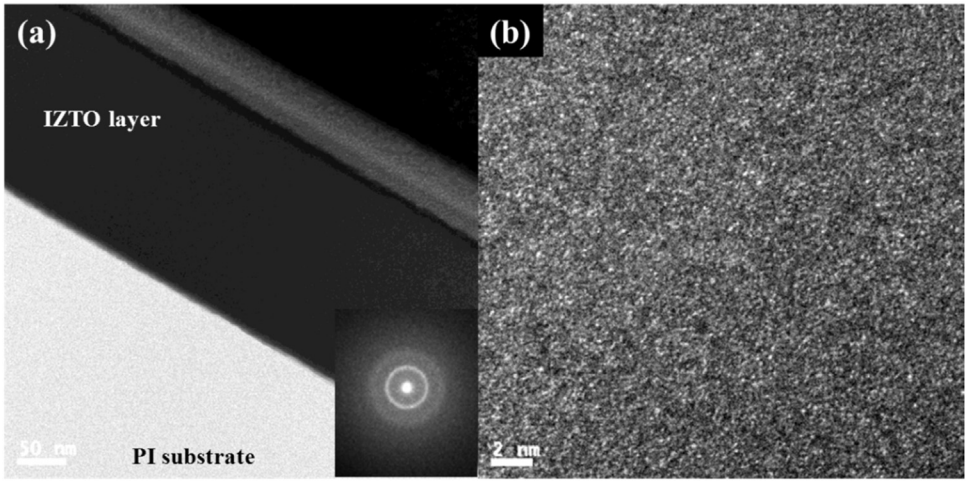

Fig. 4. (a) Cross-sectional HRTEM image of the IZTO film (inset: SAED pattern), and (b) bright-field image obtained from an IZTO film (deposition temperature: 150 °C) grown on a PI substrate.

depicted an amorphous IZTO thin film prepared on a PI substrate, matching with the surface morphology of the sample obtained through XRD analysis, SEM, and AMF images. The diffuse rings in the SAED patterns (Fig. 4(a)) confirmed the amorphous structure. The bright-field images of the IZTO film shown in Fig. 4(b) could also be described as amorphous structures although no distinct features were seen in the images. These findings suggested that the degree of surface roughness achieved in the sample could result in a more stable and effective performance of the FED, compared to that of an FED using ITO.

Fig. 5 reveals the resistivity, mobility, and the carrier concentration of the IZTO thin films fabricated at different deposition temperatures, using a Hall measurement system and a 4-point probe measuring system. As the deposition temperature rises, the resistivity of the amorphously structured IZTO thin film increases accordingly. However, at 200 °C or higher, the resistivity of the poly-crystalline IZTO thin film decreases. Therefore, the lowest resistivity of IZTO thin film is found from RT–50 °C and at 300 °C of the deposition temperature. To have a better understanding of this pattern, it is necessary to consider the generation of charge carriers in thin films. The electrical charge carrier generation of the amorphous IZTO thin films can be explained by the following two aspects: first, despite the amorphous IZTO films, the substituted Sn^{4+} at the In^{3+} site in the locally orderedregion of

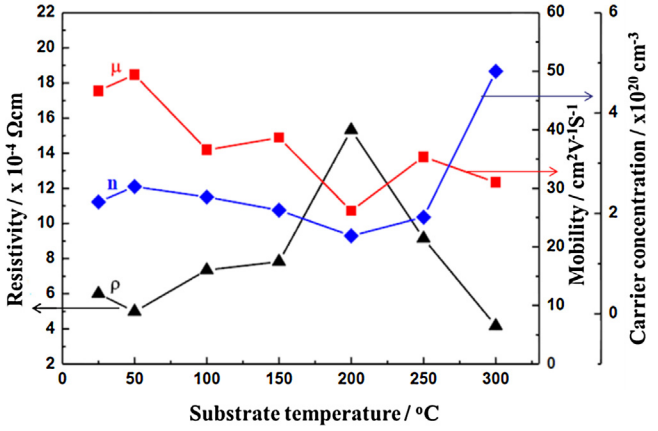

Fig. 5. Variations of the resistivity, the mobility and the carrier concentration of the IZTO films at various deposition temperatures.

the amorphous matrix can be effective as a dopant and contribute to the electrical charge carriers of the degenerated n-type semiconductor [27]. In addition, a high deficiency of oxygen generated by the Zn and Sn unintentionally doped in the In_2O_3 has the characteristics of an n-type semiconductor, generating doubly charged oxygen vacancies [32]. In this study, only deposition temperature was changed, with the doping concentration of Zn and Sn fixed to optimize the resistivity of the IZTO thin film. In the process of being deposited on the PI substrate from the IZTO target, In_2O_3, ZnO, and SnO_2 lose oxygen, forming nonstoichiometric thin films. An adequate amount of oxygen gas added during sputtering promotes generation of carriers such as oxygen vacancies [33]. Our group also reported that lowest resistivity is obtained when a small amount of oxygen gas (up to 3%) is added [30]. If the reaction temperature increases when oxygen gas is supplied at a constant level, oxygen vacancies form Zn, In, Sn metal ions, and nonstoichiometric compounds, reducing carrier concentration. As a result, resistivity increases while mobility decreases. This result is obtained because scatter centres which exist in the amorphous structure as inefficient activation and oxide complexes of Sn, increase scattering, without contributing carriers [34]. When the deposition temperature is around 200 °C, the IZTO composition is in an unstable state (amorphous + crystalline), exhibiting high resistivity. However, when the temperature exceeded 200 °C, the resistivity of the IZTO thin film rapidly decreased because the amorphous IZTO film formed a poly-crystalline structure. As a result, the amorphous IZTO film deposited at temperatures from RT–50 °C showed low resistivity ($4.9 \times 10^{-4}\,\Omega$ cm), exhibiting excellent electrical properties. The resistivity of the IZTO thin film fabricated at low temperatures is comparable to the resistivity of the conventional ITO thin film fabricated at high temperatures. In contrast, the IZTO film deposited at 300 °C showed the lowest resistivity ($4.1 \times 10^{-4}\,\Omega$ cm). However, it is not suitable as a TCE for the FEDs because of the formation of a poly-crystalline structure IZTO film.

The optical transmittances of the IZTO thin films deposited at different deposition temperatures were measured using the UV-visible spectrometre, and the results are shown in Fig. 6. As the deposition temperature increased, optical transmittance also increased. This is similar to the pattern observed in TCEs that have metal oxide as a component. In case of the IZTO thin films fabricated at all conditions, 80% or higher optical transmittance was observed in the visible range of 380–780 nm, confirming a similarity with the conventional ITO thin films. To check the optical

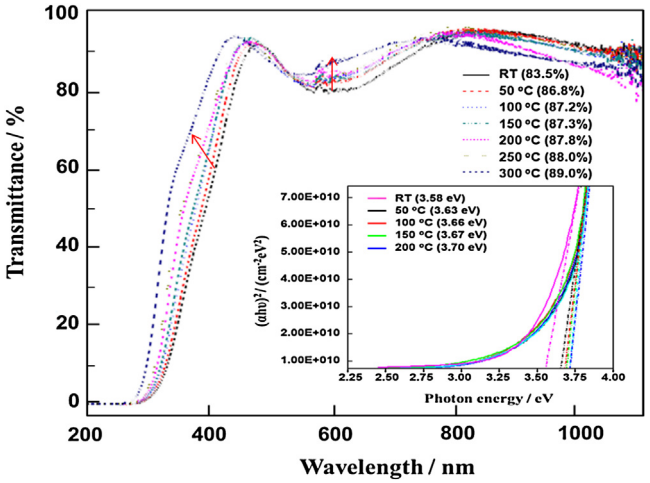

Fig. 6. Optical transmission spectra of the IZTO films grown at various deposition temperatures on PI substrates, with the inset showing the plot of $(\alpha h\upsilon)^2$ vs. photon energy for the IZTO films at various deposition temperatures.

energy band gap of the IZTO thin films with changes in deposition temperature, Fig. 6 inset shows changes in the absorption coefficient (α) with respect to the photon energy ($h\upsilon$). The optical energy band gap of the IZTO thin films is determined using Eq. (1) below [35]. Here, 'D' refers to a constant depending upon the material while 'Eg' refers to an optical band gap.

$$\alpha(h\upsilon) = D(h\upsilon - Eg)^{1}/_{2} \quad (1)$$

The calculated optical band gap of the IZTO thin films was in the range 3.58–3.70. The optical band gap sensitively changes according to oxygen partial pressure conditions during the sputtering process. Similar to most metal oxide TCEs including the ITO, based on the results in Figs. 6 and 7, as transmittance is enhanced, the optical band gap increased.

Haacke proposed a figure of merit (Φ_{TC}) value as a useful tool to compare the performances of the TCO thin films that have similar levels of optical transmittance and resistivity [36]. The Φ_{TC} value can be estimated through Eq. (2) below based on the optical transmittance (T) and the sheet resistance (R_{sh}) of the IZTO thin films, with changes in deposition temperature, and the results are shown in Fig. 7.

$$\Phi_{TC} = T^{10}/R_{sh} \quad (2)$$

As expected, the results of electro-optic properties indicated that Φ_{TC} value of the IZTO thin film was the highest at 50 °C and at

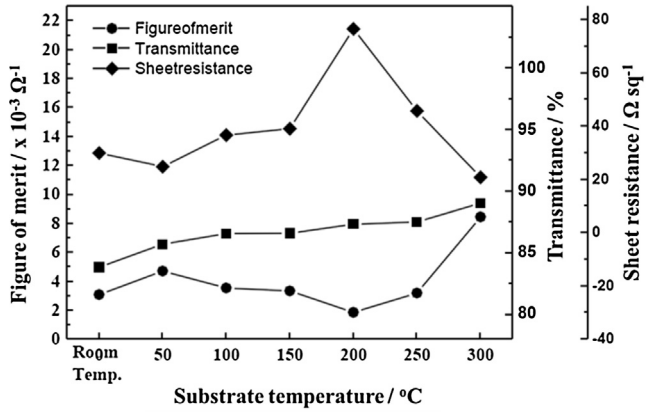

Fig. 7. Calculated figure of merit value for the IZTO films grown at various deposition temperatures.

300 °C with the increase in deposition temperature. At 300 °C, however, the IZTO has a poly-crystalline structure, but at 50 °C, close to the RT of thin films of the finest quality was obtained. In other words, when the IZTO thin film was fabricated with a supply of oxygen gas at 3%, at deposition temperatures ranging from RT to 150 °C, the IZTO film was non-crystalline, and superior-quality TCEs with significant electro-optic properties were fabricated.

Fig. 8 reveals the XPS core level spectra of O 1s, In 3d, Zn 2p, and Sn 3d. The chemical binding state of the IZTO thin films with changes in deposition temperature was analysed using XPS analysis. Despite increase in deposition temperature, no particular change was observed in the In 3d, Zn 2p, and Sn 3p peaks. As illustrated in Fig. 9(a), however, as deposition temperature increases, higher binding energies of the O 1s peaks in the IZTO thin films, decreased. Fan and Goodenough classified O 1s data into two types of O_{2-} ions: O_I and O_{II}. The higher binding energy peak (O_I) and lower binding energy peak (O_{II}) of O_{2-} are matched with the amount of oxygen vacancies and the six nearest-neighbour O_{2-} ions of the full complement neighboured with the In atoms, respectively [37]. In this study, the binding energy ratio ($I(O_I)/I(O_{II})$) of the IZTO thin films were 1.87, 1.75, 1.72, 1.65, and 1.72 respectively, when the deposition temperature was RT, 50, 100, 150, and 200 °C. When the deposition temperature was 200 °C, however, the binding energy ratio increased because of the oxide complexes formed by excessive oxygen vacancies. However, the pattern of O 1s peak intensity at RT–150 °C matched with the results of the electrical carrier concentration shown in Fig. 5. Therefore, it is confirmed that the electrical carrier concentration of the IZTO thin film is closely related to the peak ratio ($I(O_I)/I(O_{II})$) of O 1s observed through the XPS.

The work function of the IZTO thin films at different deposition temperatures was measured using the inelastic secondary electron cut-off of the UPS energy distribution at an ultrahigh vacuum state, and the results are illustrated in Fig. 9. Sugiyama et al. reported that the work function of the doped In_2O_3 thin film could be influenced by surface contamination, oxygen status, and dopant concentration. If surface oxygen concentration increases, the work function could improve [38]. In this study, the dopant concentration was fixed at the deposition of the IZTO thin film. The work function of the IZTO thin film fabricated under diverse deposition temperature conditions is primarily influenced by the oxygen vacancies that form donor states. In the electro-optically stable IZTO thin films, therefore, as the deposition temperature increases, oxygen vacancies are removed, strengthening the work functions. This result matches with the changes in the electrical carrier concentration and the XPS O 1s peak ratio. The work function of the IZTO thin films fabricated under diverse deposition temperature conditions was at least 5.3 eV, exhibiting a relatively high value compared to the conventional ITO (up to 4.7 eV). Hence, it is anticipated that the properties of the fabricated devices would be enhanced owing to a low hole-injection barrier between the work function of the IZTO thin film and the HOMO level of the emitting layer materials.

Fig. 10 shows the inner and outer bending tests of the flexible IZTO thin films and their results with changes in deposition temperature. As shown in Fig. 10(a), if the deposition temperature increases, the outer bending radius decreases. When thermally treated at 150 °C, a minimum bending radius of 4 mm was found. Thereafter, the IZTO revealed a poly-crystalline structure, and the bending radius increased. Unlike an outer bending test, as the deposition temperature rises, the bending radius increases in an inner bending test (Fig. 10(b)). This can be elaborated by Fig. 10(c) that shows the results of the measurement of residual stress versus the deposition temperature. Based on these results, as the deposition temperature increases, compressive stress was found on the PI substrate and the IZTO. Therefore, tensile stress that

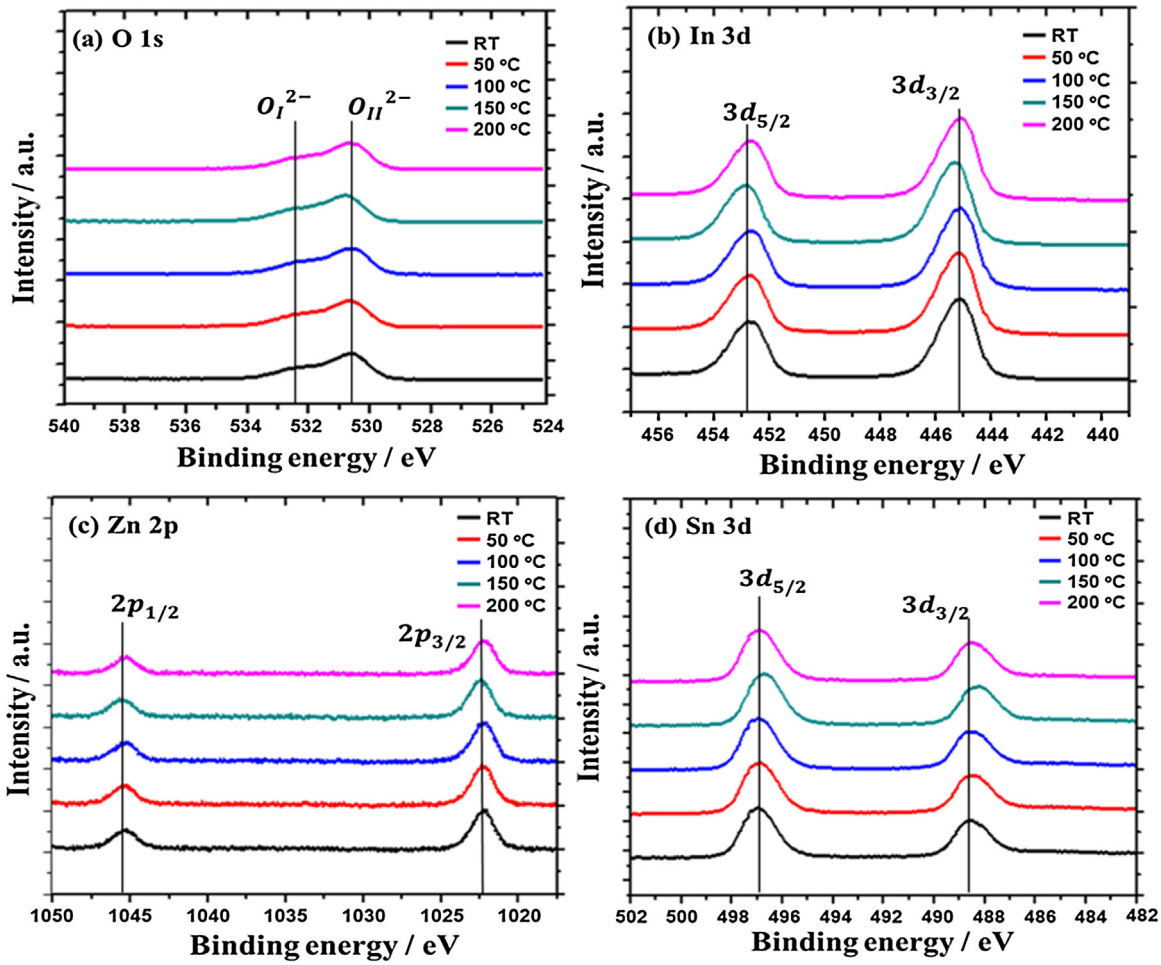

Fig. 8. XPS core level spectra of (a) O 1s, (b) In 3d, (c) Zn 2p, and (d) Sn 3d obtained for IZTO films grown on a PI substrate, as a function of various deposition temperatures.

occurs at outer bending is offset by rising compressive stress as the deposition temperature increases. At inner bending, however, compressive stress becomes more intense, and the bending radius increases. Hence, at an outer bending test, a minimum bending radius of 2.8 mm was found at RT conditions.

Fig. 11(a) and (b) shows the brightness-voltage and luminance efficiency-current density of the flexible IZTO PLEDs respectively, and the results are stated in Table 1. In the flexible IZTO PLED fabricated at 100 °C of deposition temperature, the maximum brightness was 22,860 cd/cm^2 at 9 V. In addition, high luminance efficiency at low current density is depicted in Fig. 11(b). Therefore, power consumption could be reduced by using the IZTO in FEDs.

In general, in TCEs, if transmittance increases, electrical properties decrease (trade-off). Therefore, the optimized deposition temperature of the IZTO film can be estimated through the Φ_{TC} value that was obtained using the transmittance and the sheet resistance of the IZTO film. At a range of 50–100 °C of the IZTO, Φ_{TC} values ranged from 4.0 to 4.8. In particular, a maximum brightness and a maximum efficiency of 21,115 cd/m^2 and 6.71 cd/A respectively was exhibited by the flexible IZTO PLED to which the TCE fabricated at a deposition temperature 100 °C was applied. As the deposition temperature is below 100 °C, a plastic substrate having better transmittance than PI can be used to improve device performances.

To assess the properties of a flexible IZTO, an ITO PLED was fabricated under the same conditions as the flexible IZTO PLED, and the properties were assessed. In the ITO PLED, a TCE in which the ITO was deposited on a glass substrate was applied (fabricator, 10 Ω/sq). The maximum brightness and maximum efficiency of ITO PLED were 20,987 cd/m^2 and 5.27 cd/A, respectively. The maximum brightness and maximum efficiency of the flexible IZTO

Table 1
Characteristics of devices.

Deposition temperature [°C]	Sheet resistance [Ω/sq]	Figure of merit [10^{-3} Ω^{-1}]	Turn on voltage [V]	Max. brightness [cd/m^2]	Max. efficiency [cd/A]	CIE coordinates
RT	30	3	3.2	18,832	6.65	(0.29,0.58)
50	28	4.8	3.1	21,115	6.71	(0.29,0.58)
100	35	4.0	3.1	22,860	6.91	(0.30,0.58)
150	36	3.8	3.1	21,096	6.90	(0.31,0.58)
200	78	2	3.1	20,015	6.81	(0.30,0.58)
[a]Ref.	10	–	3.3	20,987	5.27	(0.29,0.58)

[a] ITO(170 nm)/PEDOT:PSS(40 nm)/Green polymer(80 nm)/BaF_2(2 nm)/Ba(2 nm)/Al(200 nm).

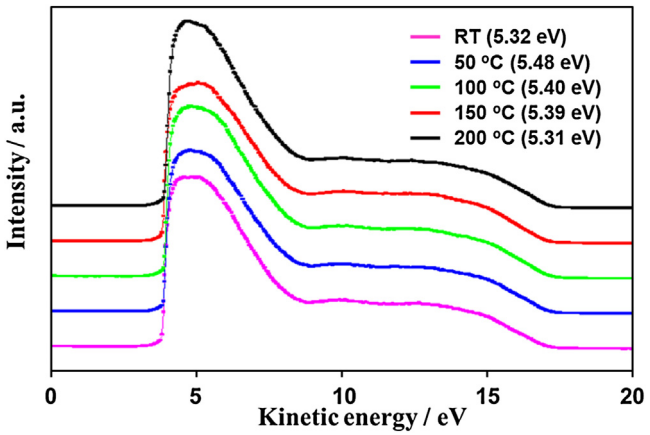

Fig. 9. Low kinetic energy cut offs of the IZTO films with UPS and the work function of the IZTO films deposited at various deposition temperatures.

PLED were greater by 9% and 31% respectively, compared to the ITO PLED. It is highly significant that a flexible IZTO PLED sputtered at a substrate annealing temperature of 100 °C or lower revealed better efficiency than an ITO sputtered at 300 °C or higher. The work function of the ITO (ca. −4.7 eV) is too low to be used as the TCO for the anode. For efficient hole injection of the emitting layer, therefore, a TCE with a high work function is required to reduce the energy barrier of the anode and the emitting layer. The flexible IZTO ranged from (ca. −5.32 eV to ca. −5.48 eV) depending upon the deposition temperature. When it is fabricated with the same device structure as the ITO, holes can be effectively injected. Because of these reasons, even though the optical and electrical properties of IZTO film were lower than the ITO, the IZTO was able to show better performances in accordance with the hole-electron balance. Introduction of the PEDOT:PSS layer to enhance the surface morphology of IZTO film, can further improve the hole transporting properties.

Table 2
Mechanical characteristics of devices.

	RT	50 °C	100 °C	150 °C	200 °C
Outer bending	4.5 mm	4.5 mm	4.3 mm	4.5 mm	4.7 mm
Inner bending	3.5 mm	4.5 mm	4.7 mm	5.0 mm	3.0 mm
Stretching	2.8%	3.2%	2.2%	1.4%	1.8%
Twisting	48°	50°	58°	50°	50°

Finally, a mechanical test on the fabricated flexible IZTO PLEDs was conducted. In addition to the inner and outer bending tests, stretching and twisting tests were performed, and the results are shown in Table 2. When the deposition temperature increased, the outer bending radius decreased, exhibiting a minimum bending radius of 4.3 mm at 100 °C. In an inner bending test, as deposition temperature increased, the bending radius increased, exhibiting a maximum bending radius of 5.0 mm of at 150 °C. This study confirmed that as the deposition temperature rises, the compressive stress of the PI substrate and the IZTO become more intense, through analysis of the residual stress of the IZTO film. Therefore, tensile stress that occurs at outer bending is offset by the compressive stress that increases as deposition temperature

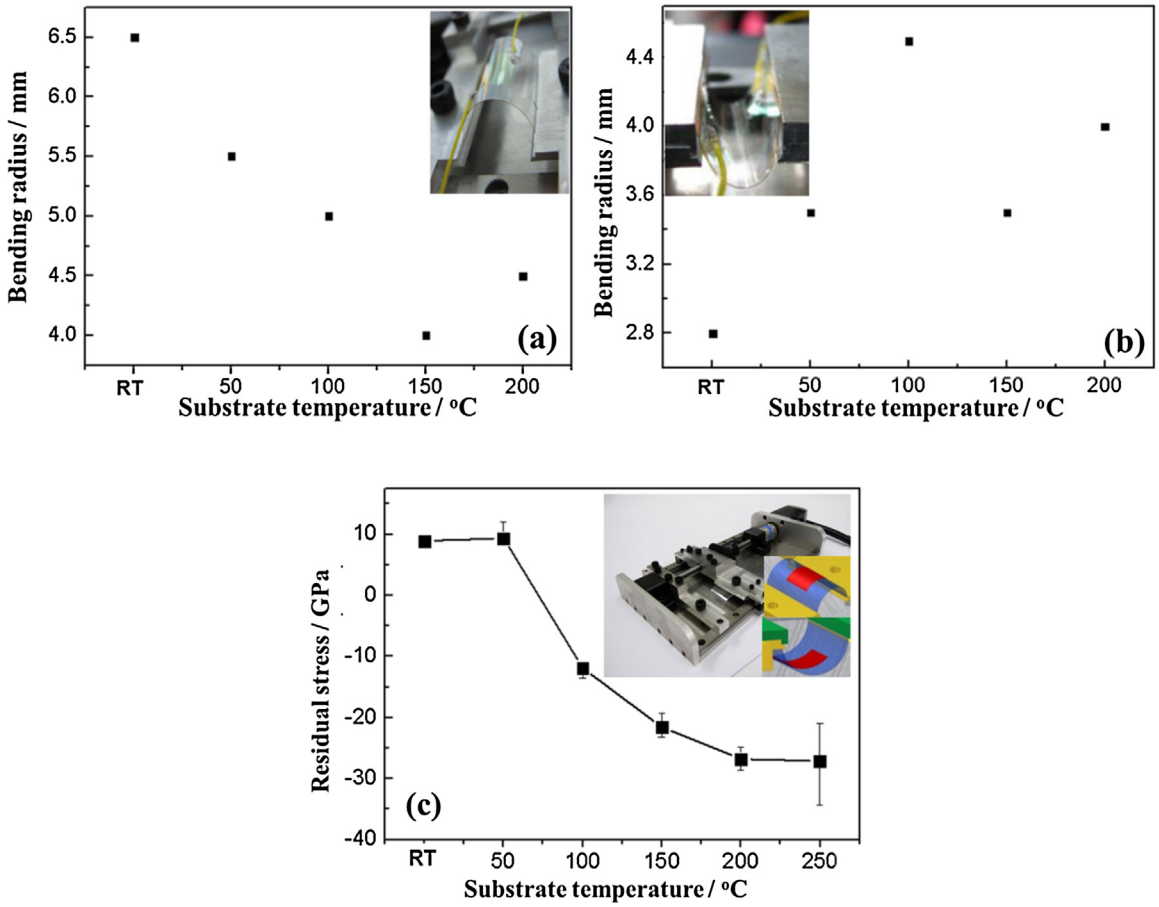

Fig. 10. Mechanical test of the flexible IZTO films at various deposition temperatures, (a) outer bending test, (b) inner bending test, and (c) residual stress test. Inset showing the methods for the various mechanical tests.

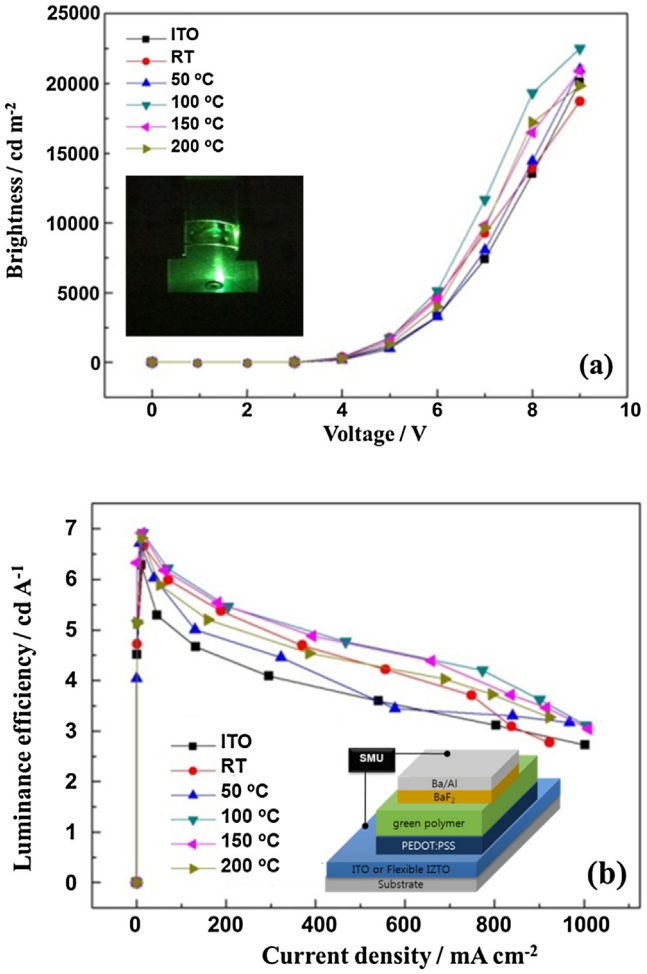

Fig. 11. (a) Brightness—voltage characteristics of PLEDs using IZTO films with various deposition temperatures. (Inset: luminescence image of flexible IZTO PLEDs), and (b) efficiency—current density characteristics of PLEDs using an IZTO films at various deposition temperatures. (Inset: device structures of PLEDs).

rises. At inner bending, however, the bending radius increases because of increased compressive stress. Therefore, it was confirmed that flexible IZTO PLEDs reveal similar mechanical characteristics as the IZTO film. However, because of the multiple influence of the PEDOT:PSS, green polymer, inorganic buffer layer, and the metal electrode deposited on the IZTO film, compressive stress on the flexible IZTO PLED increases, and the decrease in outer bending radius is greater than the IZTO film. In contrast, inner bending radius increases. To test durability under diverse circumstances for improvement of portability, some more stretching and twisting tests were carried out. The PLED to which the IZTO film fabricated at 50 °C was applied, showed 3.2% stretching stability. Further, the PLED to which the IZTO film fabricated at 100 °C was applied, operated normally despite being twisted by 58°. The said results indicate that IZTO films fabricated at 150 °C or below demonstrate excellent device performance and mechanical stability. In addition, similarity with the results predicted through the figure of merit of the IZTO films, was also confirmed.

Conclusion

In this study, we manufactured an IZTO target by reducing the indium content 15% below than that used for ITO. The IZTO target was manufactured with a composition of 70 at.% In_2O_3– 15 at.% ZnO^- 15 at.% SnO_2, and FIZTO films were formed on a polyimide film at various temperatures, ranging from RT–300 °C with an oxygen partial pressure of 3% using a pulsed DC magnetron sputtering system. Amorphous FIZTO film prepared at a temperature of 50 °C showed the best performance. The largest figure of merit of $4.8 \times 10^{-3}\ \Omega^{-1}$ was obtained with an optical transmittance of 86.8%, a sheet resistance of 28 Ω/sq and work function of 5.48 eV. The inner bending and the outer bending radius of the FIZTO film was 4.0 mm and 2.8 mm, respectively. The FPLEDs with the FIZTO film deposited under optimum conditions exhibited a maximum brightness and a maximum luminance efficiency of 21,115 cd/cm^2 and 6.71 cd/A, respectively, with a 31% and 9% enhancement in device performance compared to PLEDs with a commercial ITO glass. In addition, the FPLEDs demonstrated significant flexibility in the stretching and twisting tests, with a stretching stability of 3.2% and worked normally in a twisted state at 58°.

Acknowledgements

This work was supported by the Energy Efficiency & Resources Core Technology Program of the KETEP, granted financial resource from the Ministry of Trade, Industry & Energy, Republic of Korea. (No. 20142020103970) and New & Renewable Energy Core Technology Program of the Korea Institute of Energy Technology Evaluation and Planning (KETEP), grant financial resource from the Ministry of Trade, industry & Energy, Republic of Korea (No. 20153010140030).

References

[1] R.H. Friend, R.W. Gymer, A.B. Holmes, J.H. Burroughes, R.N. Marks, C. Taliani, D.D.C. Bradley, D.A. Dos Santos, J.L. Bredas, M. Logdlund, W.R. Salaneck, Nature 397 (6715) (1999) 121, doi:http://dx.doi.org/10.1038/16393.
[2] K. Zhang, Z. Hu, R. Xu, X.-F. Jiang, H.-L. Yip, F. Huang, Y. Cao, Adv. Mater. 27 (24) (2015) 3607, doi:http://dx.doi.org/10.1002/adma.201500972.
[3] S. Höfle, A. Schienle, C. Bernhard, M. Bruns, U. Lemmer, A. Colsmann, Adv. Mater 26 (30) (2014) 5155, doi:http://dx.doi.org/10.1002/adma.201400332.
[4] W. Qin, Z. Yang, Y. Jiang, J.W.Y. Lam, G. Liang, H.S. Kwok, B.Z. Tang, Chem. Mater. 27 (11) (2015) 3892, doi:http://dx.doi.org/10.1021/acs.chemmater.5b00568.
[5] S. Kwon, C. Kim, S. Kim, S.H. Han, Int. J. Ind. Ergon. 40 (6) (2010) 733, doi:http://dx.doi.org/10.1016/j.ergon.2010.06.006.
[6] J. Jean, S. Chang, P.R. Brown, J.J. Cheng, P.H. Rekemeyer, M.G. Bawendi, S. Gradečak, V. Bulović, Adv. Mater. 25 (20) (2013) 2790, doi:http://dx.doi.org/10.1002/adma.201204192.
[7] D.C.J. Neo, C. Cheng, S.D. Stranks, S.M. Fairclough, J.S. Kim, A.I. Kirkland, J.M. Smith, H.J. Snaith, H.E. Assender, A.A.R. Watt, Chem. Mater. 26 (13) (2014) 4004, doi:http://dx.doi.org/10.1021/cm501595u.
[8] M.H. Choi, K.W. Song, D.K. Moon, J.R. Haw, J. Ind. Eng. Chem. 29 (2015) 120, doi:http://dx.doi.org/10.1016/j.jiec.2015.03.024.
[9] M.-H. Choi, K.W. Song, D.K. Moon, Polym. Chem. 6 (14) (2015) 2636, doi:http://dx.doi.org/10.1039/C5PY00003C.
[10] S.W. Heo, K.W. Song, D.K. Moon, RSC Adv. 4 (13) (2014) 6776, doi:http://dx.doi.org/10.1039/c3ra42263a.
[11] S.W. Heo, E.J. Lee, K.W. Seong, D.K. Moon, Sol. Energy Mater. Sol. Cells 115 (2013) 123.
[12] J. Szczyrbowski, K. Schmalzbauer, H. Hoffmann, Thin Solid Films 137 (2) (1986) 169, doi:http://dx.doi.org/10.1016/0040-6090(86)90017-9.
[13] K.L. Chopra, S. Major, D.K. Pandya, Thin Solid Films 102 (1) (1983) 1, doi:http://dx.doi.org/10.1016/0040-6090(83)90256-0.
[14] Y. Shen, D.B. Jacobs, G.G. Malliaras, G. Koley, M.G. Spencer, A. Ioannidis, Adv. Mater. 13 (16) (2001) 1234, doi:http://dx.doi.org/10.1002/1521-4095(200108)13:16<1234:AID-ADMA1234>3.0.CO;2-R.
[15] X. Hu, L. Chen, Y. Zhang, Q. Hu, J. Yang, Y. Chen, Chem. Mater. 21 (26) (2014) 6293, doi:http://dx.doi.org/10.1021/cm5033942.
[16] D.R. Cairns, R.P. Witte, D.K. Sparacin, S.M. Sachsman, D.C. Paine, G.P. Crawford, R.R. Newton, Appl. Phys. Lett. 76 (11) (2000) 1425, doi:http://dx.doi.org/10.1063/1.126052.
[17] K.A. Sierros, N.J. Morris, S.N. Kukureka, D.R. Cairns, Wear 267 (1–4) (2009) 625, doi:http://dx.doi.org/10.1016/j.wear.2008.12.042.
[18] K.A. Sierros, N.J. Morris, K. Ramji, D.R. Cairns, Thin Solid Films 517 (8) (2009) 2590, doi:http://dx.doi.org/10.1016/j.tsf.2008.10.031.
[19] G.J. Exarhos, X.-D. Zhou, Thin Solid Films 515 (18) (2007) 7025, doi:http://dx.doi.org/10.1016/j.tsf.2007.03.014.
[20] T. Minami, MRS Bull. 25 (8) (2011) 38, doi:http://dx.doi.org/10.1557/mrs2000.149.
[21] T. Minami, Semicond. Sci. Technol. 20 (4) (2005) S35, doi:http://dx.doi.org/10.1088/0268-1242/20/4/004.

[22] T. Minami, Thin Solid Films 516 (7) (2008) 1314, doi:http://dx.doi.org/10.1016/j.tsf.2007.03.082.
[23] T. Minami, Thin Solid Films 516 (17) (2008) 5822, doi:http://dx.doi.org/10.1016/j.tsf.2007.10.063.
[24] X. Li, T.-Y. Zhang, Y.J. Su, Nano Lett. 15 (8) (2015) 4883, doi:http://dx.doi.org/10.1021/acs.nanolett.5b00399.
[25] N. Atar, E. Grossman, I. Gouzman, A. Bolker, V.J. Murray, B.C. Marshall, M. Qian, T.K. Minton, Y. Hanein, ACS Appl. Mater. Interfaces 7 (22) (2015) 12047, doi:http://dx.doi.org/10.1021/acsami.5b02200.
[26] X. Pan, Y. Zhao, S. Liu, C.L. Korzeniewski, S. Wang, Z. Fan, ACS Appl. Mater. Interfaces 4 (8) (2012) 3944, doi:http://dx.doi.org/10.1021/am300772t.
[27] J.M. Phillips, R.J. Cava, G.A. Thomas, S.A. Carter, J. Kwo, T. Siegrist, J.J. Krajewski, J.H. Marshall, W.F. Peck, D.H. Rapkine, Appl. Phys. Lett. 67 (15) (1995) 2246, doi:http://dx.doi.org/10.1063/1.115118.
[28] T. Minami, T. Yamamoto, Y. Toda, T. Miyata, Thin Solid Films 373 (1–2) (2000) 189, doi:http://dx.doi.org/10.1016/S0040-6090(00)01132-9.
[29] C.A. Hoel, T.O. Mason, J.-F. Gaillard, K.R. Poeppelmeier, Chem. Mater. 22 (12) (2010) 3569, doi:http://dx.doi.org/10.1021/cm1004592.
[30] S.W. Heo, Y.D. Ko, Y.S. Kim, D.K. Moon, J. Mater. Chem. C 1 (42) (2013) 7009, doi:http://dx.doi.org/10.1039/c3tc30789a.
[31] B. Yaglioglu, H.Y. Yeom, R. Beresford, D.C. Paine, Appl. Phys. Lett. 89 (6) (2006) 62103, doi:http://dx.doi.org/10.1063/1.2335372.
[32] C.W. Ow-Yang, H. Yeom, D.C. Paine, Thin Solid Films 516 (10) (2008) 3105, doi:http://dx.doi.org/10.1016/j.tsf.2007.07.205.
[33] L.-J. Meng, J. Gao, R.A. Silva, S. Song, Thin Solid Films 516 (16) (2008) 5454, doi:http://dx.doi.org/10.1016/j.tsf.2007.07.071.
[34] J.R. Bellingham, W.A. Phillips, C.J. Adkins, J. Phys. Condens. Matter 2 (28) (1990) 6207, doi:http://dx.doi.org/10.1088/0953-8984/2/28/011.
[35] S.T. Tan, B.J. Chen, X.W. Sun, W.J. Fan, H.S. Kwok, X.H. Zhang, S.J. Chua, J. Appl. Phys. 98 (1) (2005) 13505, doi:http://dx.doi.org/10.1063/1.1940137.
[36] G. Haacke, J. Appl. Phys. 47 (9) (1976) 4086, doi:http://dx.doi.org/10.1063/1.323240.
[37] J.C.C. Fan, J.B. Goodenough, J. Appl. Phys. 48 (8) (1977) 3524, doi:http://dx.doi.org/10.1063/1.324149.
[38] K. Sugiyama, H. Ishii, Y. Ouchi, K. Seki, J. Appl. Phys 87 (1) (2000) 295, doi:http://dx.doi.org/10.1063/1.371859.